

Is there a fundamental acceleration scale in galaxies?

Zhe Chang,^{1,2} Yong Zhou^{1,2*}

¹*Institute of High Energy Physics, Chinese Academy of Sciences, Beijing 100049, China*

²*School of Physical Sciences, University of Chinese Academy of Sciences, Beijing 100049, China*

Accepted XXX. Received YYY; in original form ZZZ

ABSTRACT

Milgrom’s modified Newtonian dynamics (MOND) can explain well the mass discrepancy problem in galaxy without invoking dark matter. The MOND theory predicts a universal constant acceleration scale in galaxy, below which the Newtonian dynamics is no longer valid. Recently, Rodrigues et al. analyzed 193 high-quality disk galaxies by using Bayesian inference and they concluded that the probability of existence of a fundamental acceleration scale is essentially 0. In this paper, we use the same method to revisit the same question: Is there a fundamental acceleration scale in galaxies? We fit each galaxy rotation curve of 175 SPARC galaxies with Gaussian priors on galaxy parameters and a variable acceleration scale. After marginalizing over the nuisance parameters, we find that the marginalized posterior distributions of the acceleration scale become broad. The incompatibility between the global best fit and the marginalized posterior distributions of the acceleration scale is greatly reduced. However, there still exists evidence that rejects MOND as a fundamental theory. More accurate observations are needed to exclude or confirm the existence of a fundamental acceleration scale in galaxies.

Key words: galaxies: fundamental parameters – galaxies: kinematics and dynamics

1 INTRODUCTION

In galactic scale, the mass discrepancy problem (Rubin et al. 1978; Bosma 1981) has been found for many years. The approximately flatness of rotation curves in disk galaxies is faster than that expected from the luminous matter (stellar and gas). Therefore, it seems that there needs a significant amount of non-luminous matter, i.e. the dark matter in galaxy system. As the cornerstone of the the standard cosmological paradigm (Λ CDM), there are many strong indirect evidences that support the existence of dark matter. But up to now, no direct evidence of its existence has been found (Akerib et al. 2017; Aprile et al. 2017; Cui et al. 2017). A successful alternative to the dark matter hypothesis is the modified Newtonian dynamics (MOND, Milgrom 1983; Sanders & McGaugh 2002; Famaey & McGaugh 2012), which attributes the mass discrepancy in galaxy system to a departure from the Newtonian dynamics at low accelerations. According to the MOND, the Newtonian dynamics is modified as the form,

$$\mathbf{a}_N = \mu\left(\frac{a}{a_0}\right)\mathbf{a} \quad \text{or} \quad \mathbf{a} = \nu\left(\frac{a_N}{a_0}\right)\mathbf{a}_N, \quad (1)$$

where \mathbf{a}_N is the Newtonian acceleration, \mathbf{a} is the kinematic acceleration, $\mu(x)$ or $\nu(y)$ is the interpolating function. The interpolating functions obey the relation $\mu(x)\nu(y) = 1$ and have a characteristic acceleration scale a_0 . The MOND theory predicts the acceleration scale with $a_0 = 1.2 \times 10^{-13} \text{ km s}^{-2}$, and there have two different asymptotic behaviors around this value. In the Newton region $a \gg a_0$, the Newtonian dynamics is recovered and $a = a_N$. In the deep-MOND region $a \ll a_0$, the Newtonian dynamics is invalid and $a = \sqrt{a_0 a_N}$. With an assumed constant acceleration scale, the MOND can explain well the flat rotation curves in outer part of disk galaxies. In particular, it naturally deduces the well known global scaling relation, the Tully-Fisher relation (Tully & Fisher 1977; McGaugh et al. 2000; Lelli et al. 2016b). Although many astronomical observations on disk galaxy show a universal constant acceleration scale, whether the acceleration scale is a fundamental constant or not, is still an open question. In fact, the acceleration scale is treated as a free parameter to fit the galaxy rotation curve, and different galaxy may somehow have different acceleration scale (Begeman et al. 1991; Swaters et al. 2010; Chang et al. 2013).

Recently, Rodrigues et al. (2018b, hereafter R18) analyzed 193 high-quality disk galaxies by using Bayesian inference and they concluded that the probability of existence of a fundamental acceleration scale is essentially 0. In par-

* E-mail: zhouyong@ihep.ac.cn

ticular, the MOND theory is ruled out as a fundamental theory for galaxies at more than 10σ . However, their conclusions were built on flat priors on the galaxy parameters. The observational uncertainties of galaxy distance and inclination have been ignored (McGaugh et al. 2018; Kroupa et al. 2018), which have significant impact on the distribution of acceleration scale. It is interesting to note that there has been another study (Li et al. 2018, hereafter L18) that analyzed the same SPARC galaxy sample but found almost the opposite conclusion. They used an excessively strong Gaussian prior on acceleration scale which limits the variation of acceleration scale within a narrow region. The result based on a flat prior on acceleration scale is excluded by comparing the cumulative distributions functions (CDF) of reduced χ^2 . This method was doubted by Rodrigues et al. (2018a). In this paper, we use Bayesian inference to revisit the same question: Is there a fundamental acceleration scale in galaxies? It is argued that before Bayesian inference, one can't ignore the already existed information about the fitted parameter or take excessively strong prior. The flat priors on galaxy parameters are improper in this analysis. We use Gaussian priors on galaxy parameters and a variable acceleration scale to fit each galaxy rotation curve of 175 SPARC galaxies. We obtain the posterior distribution of acceleration scale by marginalizing over the nuisance parameters. Then, we can compare the marginalized posterior distribution of acceleration scale for each galaxy with the global best fit of acceleration scale. If the global best fit is compatible with each galaxy, then the MOND theory could be still a fundamental theory and there exists a fundamental acceleration scale in galaxies.

The rest of this paper is organized as follows. In Section 2, we make a brief introduction to the SPARC data set. Then we introduce the Bayesian analysis, especially the choice of Gaussian priors. In Section 3, We analyse the MCMC result for galaxy NGC6195 and compare it with that from R18 and L18. Then we compare the marginalized posterior distribution of acceleration scale for each galaxy with the global best fit of acceleration scale. Finally, conclusions and discussions are given in Section 4.

2 METHODOLOGY

2.1 SPARC data set

The *Spitzer* Photometry and Accurate Rotation Curves (SPARC) data set¹ (Lelli et al. 2016a) is a sample of 175 disk galaxies with new surface photometry at $3.6 \mu\text{m}$ and high-quality rotation curves from previous HI/H α studies. The surface photometry at $3.6 \mu\text{m}$ provides the stellar mass via the mass-to-light ratio conversion factor. The gas mass is provided by the 21cm observations. Most of galaxies have disk component, only a few of galaxies have extra bulge component, both of them constitute the stellar component. In total, the galaxy baryonic mass profile comprises disk, bulge and gas component and we consider no dark matter. In SPARC data set, the mass profile is represented by velocity at a given radius, so the total baryonic velocity is

$$V_{bar}^2 = \Upsilon_d V_{disk}^2 + \Upsilon_b V_{bulge}^2 + V_{gas}^2, \quad (2)$$

¹ <http://astroweb.cwru.edu/SPARC/>

where Υ_d and Υ_b are the mass-to-light ratios for disk and bulge component, respectively. According to the MOND theory, the theoretical centripetal acceleration is tightly correlated with the total baryonic mass profile,

$$g_{th} = \frac{g_{bar}}{1 - e^{-\sqrt{g_{bar}/a_0}}}, \quad \text{RAR-inspired,} \quad (3)$$

$$g_{th} = g_{bar} \cdot \left(\frac{1}{2} + \sqrt{\frac{a_0}{g_{bar}} + \frac{1}{4}} \right), \quad \text{Simple,} \quad (4)$$

$$g_{th} = g_{bar} \cdot \sqrt{\frac{1}{2} + \sqrt{\frac{a_0^2}{g_{bar}^2} + \frac{1}{4}}}, \quad \text{Standard,} \quad (5)$$

where $g_{bar} = V_{bar}^2/R$ is the baryonic acceleration and the acceleration scale a_0 is treated as a free parameter to investigate its variation from galaxy to galaxy. The RAR-inspired, simple and standard interpolating functions are used here, respectively. The RAR-inspired one comes from the radical acceleration relation (RAR) (McGaugh et al. 2016) and the simple and standard interpolating functions are mostly used in early study on fitting galaxy rotation curves (McGaugh 2008; Famaey & McGaugh 2012; Hees et al. 2016). Then we can deduce the theoretical rotation curve at every radius,

$$V_{th} = \sqrt{R \cdot g_{th}}. \quad (6)$$

Thus, we can compare the theoretical rotation curve with the observed rotation curve V_{obs} .

For individual galaxy, there are five factors that could affect the galaxy rotation curve. First, the stellar mass-to-light ratio Υ_* could affect the total baryonic matter profile and then affect the theoretical rotation curve V_{th} . Second, uncertainties in galaxy distance affect the radius and the mass profile of baryonic components. If the galaxy distance D is changed to $D' = D\delta_D$, where δ_D is a dimensionless distance factor, then the radius changes according to $R' = R\delta_D$ and the baryonic component velocity changes to $V'_k = V_k\sqrt{\delta_D}$, where k denotes disk, bulge or gas. Third, uncertainties in galaxy inclination only affect the observed rotation curves and its uncertainties. If the galaxy inclination i is changed to $i' = i\delta_i$, where δ_i is a dimensionless inclination factor, the observed rotation curves and its uncertainties change according to $V'_{obs} = V_{obs} \sin(i)/\sin(i')$ and $\delta V'_{obs} = \delta V_{obs} \sin(i)/\sin(i')$. Fourth, even the MOND theory predicts a universal constant acceleration scale, we treat the acceleration scale as a free parameter which affects the value of interpolating function $\nu(y)$ and then affects the theoretical rotation curve V_{th} . Fifth, the different interpolating function in equation (3-5) also affects theoretical rotation curve V_{th} . More details could be found in L18 or R18. An example of galaxy rotation curve for galaxy NGC6195 is shown in Fig. 3.

2.2 Bayesian analysis

In order to fit the rotation curve for individual galaxy, we implement the Bayesian inference by using the affine-invariant Markov chain Monte Carlo (MCMC) ensemble sampler in *emcee* (Foreman-Mackey et al. 2013). The posterior probability of parameter space is $P(a_0, \Upsilon_d, \Upsilon_b, \delta_D, \delta_i | SPARC) = \mathcal{L}(a_0, \Upsilon_d, \Upsilon_b, \delta_D, \delta_i | SPARC)P(a_0, \Upsilon_d, \Upsilon_b, \delta_D, \delta_i)$, where the likelihood is derived from the χ^2 function, $\mathcal{L} \sim e^{-\chi^2/2}$

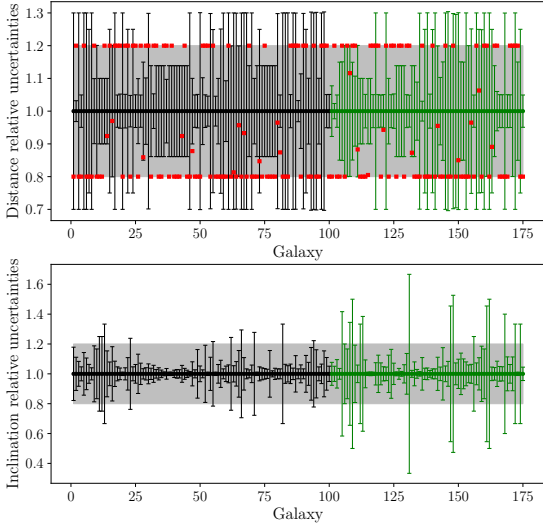


Figure 1. The relative uncertainties of galaxy distance and inclination for 175 SPARC galaxies. The first 100 galaxies are selected by 5 σ quality criteria in R18. The shaded regions represent relative uncertainty within 20%. The red dots mark the best fitting values of distance factor obtained from the minimization of χ^2 in R18.

and

$$\chi^2 = \sum_{k=1}^N \left(\frac{V_{th}(R_k; a_0, \Upsilon_d, \Upsilon_b, \delta_D) - V'_{obs,k}}{\delta V'_{obs,k}} \right)^2, \quad (7)$$

where N is the number of data point for individual galaxy, the observed rotation curve and its uncertainty at the radius R_k has been changed to $V'_{obs,k}$ and $\delta V'_{obs,k}$ with a dimensionless factor δ_i . The theoretical rotation curve V_{th} at the radius R_k is predicted by the MOND theory (with a given interpolating function) with given parameters $\{a_0, \Upsilon_d, \Upsilon_b, \delta_D\}$. The prior probability is the product of respective priors, $P(a_0, \Upsilon_d, \Upsilon_b, \delta_D, \delta_i) = P(a_0)P(\Upsilon_d)P(\Upsilon_b)P(\delta_D)P(\delta_i)$. Finally, we marginalize over the nuisance parameters set $\{\Upsilon_d, \Upsilon_b, \delta_D, \delta_i\}$, and the 1-d marginalized posterior of a_0 is as follow, $P(a_0|SPARC) = \int P(a_0, \Upsilon_d, \Upsilon_b, \delta_D, \delta_i|SPARC) d\Upsilon_d d\Upsilon_b d\delta_D d\delta_i$.

The Bayesian inference needs priors that account all the information about the parameter space before analyzing the SPARC data set. In previous work, L18 used Gaussian priors on galaxy parameters while R18 used flat priors and they got almost the opposite conclusion. Fig. 1 illustrates the relative uncertainties of galaxy distance and inclination for 175 SPARC galaxies. In upper panel, the relative uncertainties of galaxy distance range from 5% to 30% according to different observational methods. The shaded region represents a tolerance of 20% which is adopted as the range of fitting parameter in R18 and they found most of the best fitting values of distance factor locate at the boundary. This range regarded as a flat prior may be improper, the existed uncertainty is ignored and the truncation may affect the distribution of acceleration scale. In addition, their study

ignored the uncertainty of galaxy inclination which also affect the distribution of acceleration scale. In L18, Gaussian priors were imposed with the uncertainties of galaxy distance and inclination. In this paper, we use the same Gaussian priors on the galaxy distance and inclination factor. The same case happens to the choice of prior on the stellar mass-to-light ratio. R18 took a tolerance of a factor of 2 on the stellar mass-to-light ratio while L18 imposed a Gaussian prior accounting for the stellar population synthesis (SPS) model (Schombert & McGaugh 2014). We take the same Gaussian prior on the stellar mass-to-light ratio as L18. Before the Bayesian inference, there is no information about the acceleration scale for individual galaxy. One can't take excessively strong prior on it which limits the variation of acceleration scale within narrow region. Here we take a very weak Gaussian prior on the acceleration scale. In order to compare our result with R18 on the distribution of acceleration scale, we use the same notation that a_0 in the posterior probability stands for $\log_{10} a_0$. Specifically, the Gaussian prior on each parameter is represented as the normal distributions: $P(\delta_D) = \mathcal{N}(1, (\sigma_D/D)^2)$, $P(\delta_i) = \mathcal{N}(1, (\sigma_i/i)^2)$, $P(\Upsilon_d) = \mathcal{N}(0.5, 0.1^2)$, $P(\Upsilon_b) = \mathcal{N}(0.7, 0.15^2)$, $P(a_0) = \mathcal{N}(-12.921, 2^2)$, where $\log_{10}(1.2 \times 10^{-13}) \approx -12.921$. We also impose physical constraint on these parameters as follow: $\Upsilon_d > 0$, $\Upsilon_b > 0$, $\delta_D > 0$, $90^\circ > i\delta_i > 0^\circ$, $a_0 > 0$.

3 RESULT

We use *emcee* (Foreman-Mackey et al. 2013) to implement the Bayesian inference and initialize the MCMC chains with 100 random walkers. We run 500 steps in the burn-in phase and another 2000 steps in the production phase, which is enough for our purpose. We also check the acceptance fractions for all galaxies within the range (0.1, 0.7) as L18.

Fig. 2 shows the example of the Bayesian analysis with Gaussian priors for galaxy NGC6195 using the RAR-inspired interpolating function. The same Bayesian analysis of this galaxy is also represented in R18 and L18. In Fig. 2, we find that there is no strong correlation between the parameters when Gaussian priors are employed. It is the same with the result in Fig. A.1 of L18. But in Fig. 4 of R18 supplementary, there showed strong correlations between the parameters when flat priors were employed. The flat priors have no constraint for whole parameter space and the posterior is only determined by the likelihood, which ignore the existed uncertainties and lead to the maximum of posterior on Υ_d locating at the boundary. It also happens to other parameter, especially for the distance factor δ_D in most galaxies. The Gaussian priors which account for the existed information are more reasonable to constrain the parameter to be physical and not far from the expected value. L18 showed the Bayesian analysis with Gaussian priors for the parameter space $\{\Upsilon_d, \Upsilon_b, \delta_D, \delta_i\}$ and fixed the acceleration scale at $a_0 = 1.2 \times 10^{-13} \text{ km s}^{-2}$. Fig. 2 shows that a variable acceleration scale could reduce the variation of other parameter. The maximum of marginalized posterior is $\log_{10} a_0 = -13.115$, $\Upsilon_d = 0.325$, $\Upsilon_b = 0.714$, $\delta_D = 0.999$, $\delta_i = 1.008$. In addition, it also shows that the Gaussian prior imposed on a_0 is almost flat respect to the marginalized posterior, there is extremely weak constraint on the distribution of a_0 , which prevents a_0 too small. In Fig. 3, we show the rota-

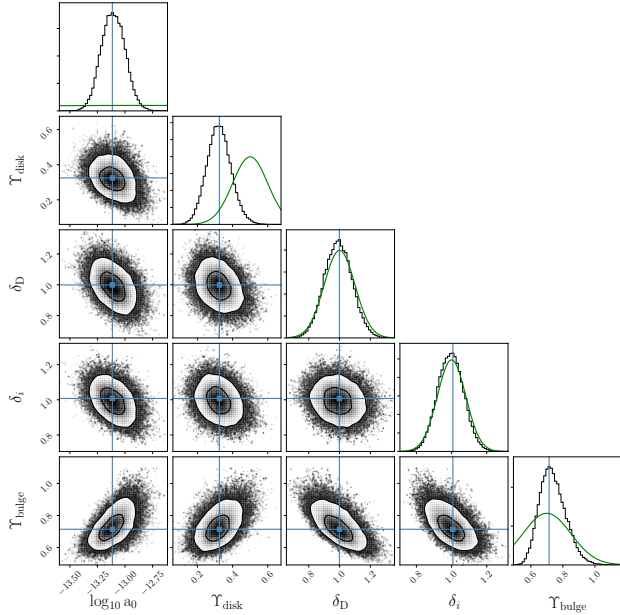


Figure 2. The 1-dimensional and 2-dimensional marginalized posteriors on the parameter space $\{\log_{10} a_0, \Upsilon_d, \Upsilon_b, \delta_D, \delta_i\}$ for galaxy NGC6195. The horizontal and vertical solid lines mark the maximum of 1-dimensional marginalized posteriors. The contours from grey to light mark 1σ and 2σ credible regions of 2-dimensional marginalized posteriors. The green lines show the prior distributions on each parameter.

tion curves for galaxy NGC6195 by using the maximum of marginalized posterior. A similar fit is obtained as well as L18.

The same Bayesian analysis with Gaussian priors for all 175 SPARC galaxies are also implemented. In order to obtain the marginalized posterior distribution of a_0 for individual galaxy, we marginalize over the nuisance parameters $\{\Upsilon_d, \Upsilon_b, \delta_D, \delta_i\}$. In R18, four quality cuts had been performed to exclude the galaxy with poor quality or poor fit. Only 100 (81) SPARC galaxies passed the 5σ (3σ) quality criteria. These quality criteria together with the maximum of marginalized posterior of a_0 and its 1σ , 3σ and 5σ confidence intervals for the RAR-inspired interpolating function are summarized in Table A1. Fig. 4 shows the marginalized posterior distributions of a_0 for those galaxies passed 5σ quality criteria. When Gaussian priors are used and the galaxy inclination is considered for the Bayesian analysis, we find that the marginalized posterior distributions of a_0 become broader than that in R18, especially for the high or low acceleration range. This feature is held for the simple and standard interpolating functions. We also perform the global best fit and estimate the confidence level in rejecting MOND as employed in R18. As shown in Fig. 4, the percentages of galaxies whose 5σ confidence intervals are incompatible with the global best fit is greatly reduced when Gaussian priors are employed. The statistical result is described in Table 1. There are only 4 galaxies comparing to 15 galaxies in R18, among the selected 100 galaxies, are incompatible with the global best fit by more than 5σ . Most of these galaxies have large acceleration scale. At low accelera-

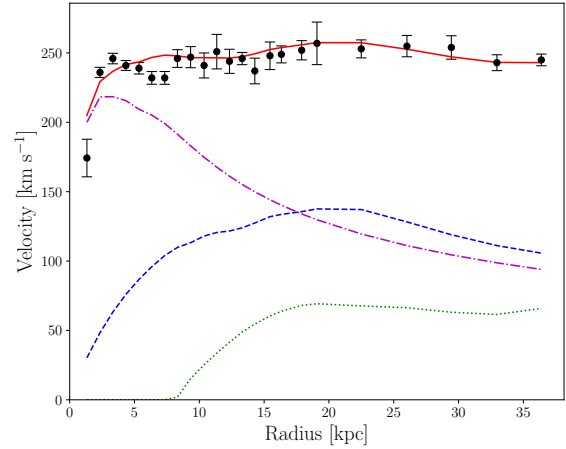


Figure 3. Example of galaxy rotation curves for galaxy NGC6195. The radius and all circular velocities have been corrected according to the maximum of 1-dimensional marginalized posteriors from Fig. 2. The points with error bars are the observed rotation curves. The solid line represents the total baryonic component velocity is represented: dotted line for the gas, dashed line for the disk, and dash-dotted line for the bulge.

tion range, those galaxies among 15 incompatible galaxies in R18 are compatible with the global best fit when Gaussian priors are employed, even though three galaxies are still incompatible for the standard interpolating function, but the discrepancy is greatly reduced. Using any of the three interpolating functions, the confidence level in rejecting MOND with Gaussian priors is nearly 25σ , about half of 50σ in R18. Fig. 5 shows the marginalized posterior distributions of a_0 for those galaxies passed 3σ quality criteria. There are only 4 galaxies, among the selected 81 galaxies, are incompatible with the global best fit by more than 5σ . The confidence level in rejecting MOND with Gaussian priors drops to 22σ , about half of 45σ in R18.

In L18, they also investigated the question whether the value of acceleration scale is truly a constant. They made Bayesian analysis with both a flat prior and a Gaussian prior on the acceleration scale. The Gaussian prior they used is $a_0 = (1.2 \pm 0.02) \times 10^{-13} \text{ km s}^{-2}$, which comes from the overall fitting of RAR for all SPARC galaxies (McGaugh et al. 2016). For individual galaxy, it may be unreasonable to take the overall fitting result as their prior. Fig. 6 shows the marginalized posterior distributions of a_0 when an excessively strong Gaussian prior on a_0 is employed. Comparing to panel a in Fig. 4, we find that the tight distribution of a_0 originates from the excessively strong Gaussian prior. By comparing the cumulative distributions functions (CDF) of reduced χ^2 (only consider the likelihood), L18 excluded the result based on the flat prior. However, the best fitting value of each parameter is obtained by maximizing the posterior, not the likelihood. As discussed in Rodrigues et al. (2018a), the CDF of the free a_0 has an advantage over the fixed a_0 when the prior is included in reduced χ^2 . Therefore, it seems

Table 1. Global best fitting values of $\log_{10} a_0$ for each interpolating function with Gaussian priors and the percentages of galaxies whose 1σ , 3σ and 5σ confidence intervals on $\log_{10} a_0$ are incompatible with the global best fit. The results of R18 with flat priors are listed as reference.

Interpolating function	Gaussian priors			Flat priors				
	$\log_{10} a_0$	1σ (32%)	3σ (0.27%)	5σ (0.000057%)	$\log_{10} a_0$	1σ (32%)	3σ (0.27%)	5σ (0.000057%)
Standard	-12.925	56%	18%	8%	-12.899	70%	33%	20%
Simple	-12.941	55%	17%	4%	-12.954	70%	34%	16%
RAR-inspired	-12.959	55%	15%	4%	-12.970	71%	31%	15%

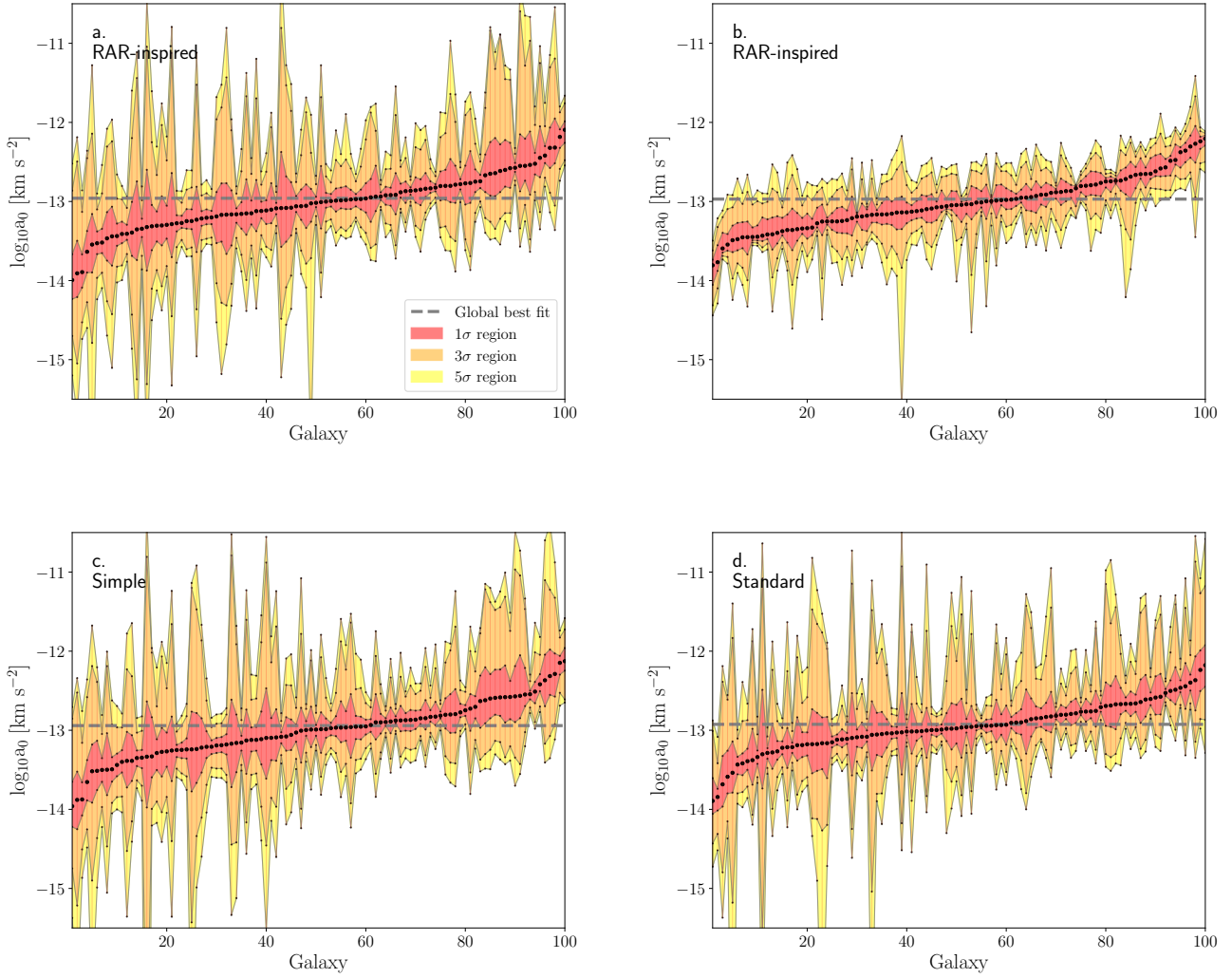


Figure 4. The marginalized posterior distributions of $\log_{10} a_0$ for the SPARC galaxies. Only 100 galaxies passed the 5σ quality criteria are displayed. The black points mark the maximum of posterior and the red, orange and yellow shaded regions are the 1σ , 3σ and 5σ confidence intervals, respectively. The grey dashed line indicates the global best fit of $\log_{10} a_0$. These galaxies are sorted by the maximum of marginalized posterior. Panels **a**, **c** and **d** respectively use the RAR-inspired, simple and standard interpolating functions with the same Gaussian priors. Panel **b** shows the result of the RAR-inspired interpolating function with flat priors in R18.

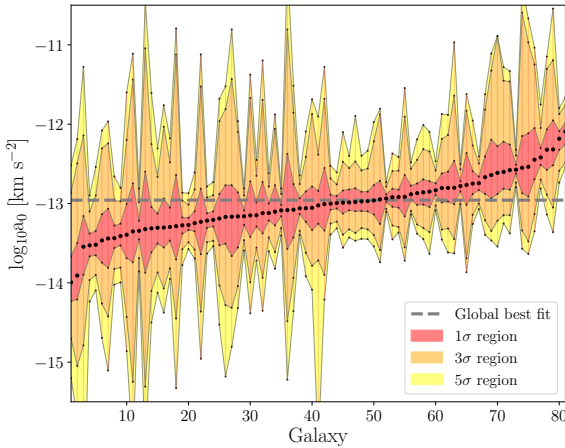


Figure 5. The marginalized posterior distributions of $\log_{10} a_0$ for the RAR-inspired interpolating function. Only 81 galaxies passed the 3σ quality criteria are displayed.

that there is still room for the variation of acceleration scale for individual galaxy.

4 CONCLUSIONS AND DISCUSSIONS

In this paper, we used Bayesian inference to revisit the question: Is there a fundamental acceleration scale in galaxies? In previous work, L18 used Gaussian priors on galaxy parameters while R18 used flat priors and they got almost the opposite conclusion. We showed that the flat priors in R18 may affect the distribution of acceleration scale a_0 . We used the same Gaussian priors on galaxy parameters as L18 and treated the acceleration scale as a free parameter to fit each galaxy rotation curve in SPARC data set. A similar fit is obtained for each galaxy rotation curve as well as L18. When Gaussian priors on galaxy parameters are used, we found that the marginalized posterior distributions of a_0 become broader than that in R18, especially for the high or low acceleration range. The incompatibility between the global best fit and the marginalized posterior distributions of a_0 is greatly reduced. These results are held for all interpolation functions we used. For the RAR-inspired interpolation function, there are only 4 galaxies comparing to 15 galaxies in R18, among the selected 100 galaxies, are incompatible with the global best fit by more than 5σ . The confidence level in rejecting MOND with Gaussian priors is nearly 25σ , about half of 50σ in R18. Besides, we found that the tight distributions of a_0 in L18 originates from the excessively strong Gaussian prior on a_0 . When the prior is included in reduced χ^2 , Rodrigues et al. (2018a) showed that the CDF of the free a_0 has an advantage over the fixed a_0 . Therefore, there is still room for the variation of a_0 for individual galaxy.

Although the Gaussian priors on galaxy parameters are employed and the incompatibility between the global best fit and the marginalized posterior distributions of a_0 is greatly reduced. There still exist evidence (about half of that in

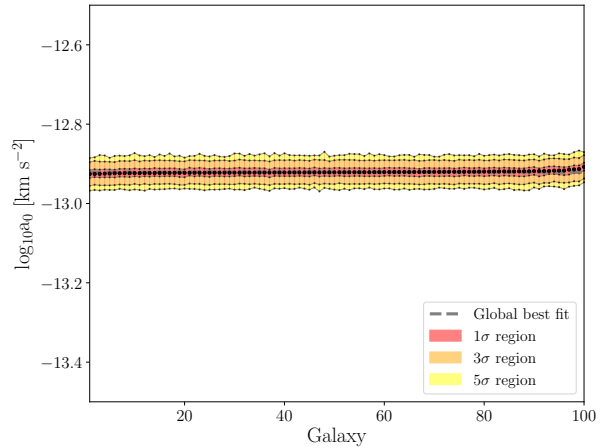


Figure 6. The marginalized posterior distributions of $\log_{10} a_0$ for the RAR-inspired interpolating function. Here we impose an excessively strong Gaussian prior $P(a_0) = \mathcal{N}(-12.921, 0.01^2)$ as same as L18.

R18) that rejects MOND as a fundamental theory. The existence of a_0 could be an emergent nature as stated in R18. In our previous work, we find the spatial distribution of a_0 could be anisotropic (Zhou et al. 2017; Chang et al. 2018), a dipole correction for a_0 could reduce the incompatibility in this paper to some extent. Furthermore, as clarified by R18, the SPARC data set are not raw observational data, they depend on galaxy surface brightness decomposition, interpretations of the inclinations and distances, assumptions on axial symmetry and choices for data binning. All of these factors could impact the SPARC data set and then impact the distribution of a_0 to some extent. More accurate observations for galaxy rotation curve and baryonic mass profile are needed to exclude or confirm the existence of a fundamental acceleration scale in galaxies.

ACKNOWLEDGEMENTS

We thank the anonymous referee for valuable suggestions and comments. We are grateful to Xin Li, Hai-Nan Lin and Zhi-Chao Zhao for useful discussions. We are also thankful for the open access of the SPARC data set. This work is supported by the National Natural Science Fund of China under grant Nos. 11675182 and 11690022.

REFERENCES

- Akerib D. S., et al., 2017, *Phys. Rev. Lett.*, 118, 021303
- Aprile E., et al., 2017, *Phys. Rev. Lett.*, 119, 181301
- Begeman K. G., Broeils A. H., Sanders R. H., 1991, *Mon. Not. Roy. Astron. Soc.*, 249, 523
- Bosma A., 1981, *Astron. J.*, 86, 1825
- Chang Z., Li M.-H., Li X., Lin H.-N., Wang S., 2013, *Eur. Phys. J.*, C73, 2447
- Chang Z., Lin H.-N., Zhao Z.-C., Zhou Y., 2018, *Chin. Phys.*, C42, 115103
- Cui X., et al., 2017, *Phys. Rev. Lett.*, 119, 181302

- Famaey B., McGaugh S., 2012, *Living Rev. Rel.*, 15, 10
- Foreman-Mackey D., Hogg D. W., Lang D., Goodman J., 2013, *Publications of the Astronomical Society of the Pacific*, 125, 306
- Hees A., Famaey B., Angus G. W., Gentile G., 2016, *Mon. Not. Roy. Astron. Soc.*, 455, 449
- Kroupa P., et al., 2018, *Nat. Astron.*, 2, 925
- Lelli F., McGaugh S. S., Schombert J. M., 2016a, *Astron. J.*, 152, 157
- Lelli F., McGaugh S. S., Schombert J. M., 2016b, *Astrophys. J.*, 816, L14
- Li P., Lelli F., McGaugh S., Schombert J., 2018, *Astron. Astrophys.*, 615, A3
- McGaugh S., 2008, *Astrophys. J.*, 683, 137
- McGaugh S. S., Schombert J. M., Bothun G. D., de Blok W. J. G., 2000, *Astrophys. J.*, 533, L99
- McGaugh S. S., Lelli F., Schombert J. M., 2016, *Physical Review Letters*, 117, 201101
- McGaugh S. S., Li P., Lelli F., Schombert J. M., 2018, *Nature Astronomy*, 2, 924
- Milgrom M., 1983, *Astrophys. J.*, 270, 365
- Rodrigues D. C., Marra V., Del Popolo A., Davari Z., 2018a, *Nat. Astron.*, 2, 927
- Rodrigues D. C., Marra V., del Popolo A., Davari Z., 2018b, *Nat. Astron.*, 2, 668
- Rubin V. C., Ford Jr. W. K., Thonnard N., 1978, *Astrophys. J.*, 225, L107
- Sanders R. H., McGaugh S. S., 2002, *Ann. Rev. Astron. Astrophys.*, 40, 263
- Schombert J., McGaugh S., 2014, *PASA*, 31, e036
- Swaters R. A., Sanders R. H., McGaugh S. S., 2010, *Astrophys. J.*, 718, 380
- Tully R. B., Fisher J. R., 1977, *Astron. Astrophys.*, 54, 661
- Zhou Y., Zhao Z.-C., Chang Z., 2017, *Astrophys. J.*, 847, 86

APPENDIX A: ADDITIONAL MATERIAL

This paper has been typeset from a $\text{\TeX}/\text{\LaTeX}$ file prepared by the author.

Table A1. The maximum of marginalized posterior of $\log_{10} a_0$ and its 1σ , 3σ and 5σ confidence intervals for the RAR-inspired interpolating function. All 175 SPARC galaxies are represented. The column P_5 (P_3) labelling with 1 indicates the galaxy passed the 5σ (3σ) quality criteria in R18.

Galaxy	P_5	P_3	$\log_{10} a_0$	$1\sigma_-$	$1\sigma_+$	$3\sigma_-$	$3\sigma_+$	$5\sigma_-$	$5\sigma_+$
CamB	0	0	-14.667	-0.272	0.335	-3.476	0.940	-6.344	1.120
D512-2	1	1	-13.230	-0.408	0.416	-1.133	1.707	-1.727	2.111
D564-8	1	1	-13.519	-0.133	0.174	-0.381	0.621	-0.576	0.980
D631-7	0	0	-13.083	-0.084	0.066	-0.215	0.237	-0.289	0.353
DDO064	1	1	-13.122	-0.255	0.393	-0.814	1.427	-1.231	1.926
DDO154	1	0	-13.017	-0.054	0.077	-0.168	0.235	-0.280	0.342
DDO161	1	1	-12.766	-0.251	0.402	-0.925	0.935	-1.100	1.145
DDO168	0	0	-13.001	-0.156	0.157	-0.400	0.551	-0.531	0.831
DDO170	1	0	-13.636	-0.262	0.263	-0.638	1.183	-0.963	1.277
ESO079-G014	1	0	-12.771	-0.267	0.224	-0.708	0.864	-0.846	1.034
ESO116-G012	1	1	-12.601	-0.211	0.379	-0.546	1.148	-0.650	1.320
ESO444-G084	1	1	-12.448	-0.245	0.398	-0.685	1.200	-0.903	1.412
ESO563-G021	0	0	-12.883	-0.087	0.087	-0.243	0.274	-0.316	0.419
F561-1	0	0	-14.495	-1.249	1.269	-4.967	4.010	-7.230	5.454
F563-1	0	0	-12.717	-0.443	0.335	-1.062	1.377	-1.506	1.840
F563-V1	0	0	-14.719	-0.832	0.745	-4.579	1.619	-7.600	2.270
F563-V2	0	0	-12.541	-0.558	0.583	-1.441	2.095	-2.253	2.540
F565-V2	1	1	-12.802	-0.206	0.339	-0.646	1.162	-0.824	1.835
F567-2	0	0	-13.657	-0.961	1.122	-4.901	3.500	-8.039	4.329
F568-1	0	0	-12.524	-0.276	0.419	-0.851	1.393	-1.148	1.955
F568-3	1	0	-13.082	-0.427	0.399	-1.004	1.551	-1.477	1.805
F568-V1	1	1	-12.550	-0.320	0.400	-0.789	1.955	-1.021	2.272
F571-8	0	0	-11.080	-0.179	0.162	-0.440	0.678	-0.546	0.854
F571-V1	1	1	-13.286	-0.418	0.646	-1.165	2.163	-2.041	2.494
F574-1	1	1	-12.962	-0.177	0.193	-0.435	0.746	-0.580	0.988
F574-2	0	0	-14.613	-1.255	0.976	-4.806	3.459	-6.615	4.597
F579-V1	0	0	-15.237	-1.120	0.892	-4.564	2.753	-6.987	3.762
F583-1	1	1	-12.916	-0.246	0.275	-0.637	1.009	-0.805	1.371
F583-4	1	1	-13.079	-0.350	0.322	-0.858	1.224	-1.279	1.563
IC2574	0	0	-13.065	-0.062	0.096	-0.169	0.330	-0.210	0.468
IC4202	0	0	-12.369	-0.262	0.380	-0.641	1.081	-0.866	1.148
KK98-251	1	1	-13.908	-0.300	0.411	-1.140	1.414	-1.791	1.720
NGC0024	1	1	-12.745	-0.086	0.082	-0.255	0.250	-0.326	0.339
NGC0055	1	1	-13.087	-0.072	0.068	-0.221	0.207	-0.315	0.279
NGC0100	1	1	-12.614	-0.266	0.337	-0.604	1.725	-0.929	1.725
NGC0247	1	0	-13.202	-0.085	0.083	-0.254	0.255	-0.345	0.359
NGC0289	1	1	-13.528	-0.138	0.148	-0.438	0.427	-0.708	0.628
NGC0300	1	1	-12.642	-0.292	0.444	-0.705	1.317	-0.824	1.531
NGC0801	0	0	-13.553	-0.058	0.056	-0.172	0.178	-0.251	0.261
NGC0891	0	0	-12.610	-0.048	0.055	-0.147	0.162	-0.183	0.264
NGC1003	0	0	-11.919	-0.327	0.354	-0.986	0.921	-1.107	0.981
NGC1090	1	0	-13.248	-0.096	0.152	-0.355	0.398	-0.447	0.644
NGC1705	0	0	-12.405	-0.095	0.107	-0.269	0.432	-0.378	0.702
NGC2366	0	0	-13.242	-0.089	0.087	-0.239	0.299	-0.328	0.558
NGC2403	0	0	-12.026	-0.093	0.076	-0.415	0.258	-0.468	0.299
NGC2683	1	1	-13.216	-0.092	0.094	-0.272	0.292	-0.414	0.430
NGC2841	1	1	-12.937	-0.043	0.052	-0.132	0.149	-0.170	0.208
NGC2903	0	0	-12.395	-0.080	0.088	-0.316	0.245	-0.377	0.285
NGC2915	1	1	-12.420	-0.095	0.119	-0.280	0.371	-0.392	0.667
NGC2955	0	0	-12.918	-0.117	0.131	-0.371	0.378	-0.485	0.593
NGC2976	0	0	-14.905	-0.975	1.164	-4.683	2.431	-7.620	2.818
NGC2998	1	0	-13.408	-0.077	0.113	-0.256	0.327	-0.353	0.468
NGC3109	0	0	-12.689	-0.077	0.076	-0.210	0.272	-0.286	0.411
NGC3198	1	0	-12.971	-0.090	0.066	-0.233	0.226	-0.283	0.319
NGC3521	1	1	-12.921	-0.120	0.107	-0.356	0.330	-0.530	0.552
NGC3726	1	0	-13.114	-0.172	0.129	-0.458	0.490	-0.593	0.724
NGC3741	1	1	-12.834	-0.057	0.089	-0.190	0.250	-0.255	0.367
NGC3769	1	1	-12.989	-0.138	0.154	-0.404	0.515	-0.568	0.889
NGC3877	0	0	-13.220	-0.261	0.308	-2.375	0.885	-5.404	1.107
NGC3893	1	1	-12.749	-0.131	0.156	-0.395	0.480	-0.509	0.796
NGC3917	1	0	-13.157	-0.187	0.148	-0.516	0.539	-0.727	0.820

Table A1 – continued

Galaxy	P_5	P_3	$\log_{10} a_0$	$1\sigma_-$	$1\sigma_+$	$3\sigma_-$	$3\sigma_+$	$5\sigma_-$	$5\sigma_+$
NGC3949	0	0	-12.893	-0.326	0.224	-1.523	0.818	-5.802	1.024
NGC3953	0	0	-13.665	-0.916	0.379	-5.107	0.698	-8.624	0.853
NGC3972	1	1	-12.803	-0.174	0.203	-0.511	0.667	-0.815	0.919
NGC3992	1	1	-13.275	-0.104	0.100	-0.301	0.313	-0.501	0.410
NGC4010	1	1	-12.805	-0.181	0.184	-0.525	0.619	-0.648	0.933
NGC4013	1	1	-12.884	-0.067	0.107	-0.210	0.321	-0.258	0.403
NGC4051	0	0	-13.586	-0.930	0.548	-5.343	1.009	-8.063	1.205
NGC4068	0	0	-13.566	-0.356	0.243	-1.146	0.954	-1.956	1.475
NGC4085	1	0	-12.788	-0.230	0.239	-0.713	0.795	-1.097	1.142
NGC4088	1	1	-13.149	-0.140	0.161	-0.409	0.498	-0.571	0.698
NGC4100	1	1	-13.206	-0.082	0.107	-0.265	0.310	-0.331	0.476
NGC4138	1	1	-13.024	-0.231	0.183	-0.693	0.639	-3.028	1.120
NGC4157	1	1	-12.970	-0.129	0.119	-0.356	0.410	-0.479	0.635
NGC4183	1	1	-13.437	-0.124	0.158	-0.388	0.473	-0.586	0.777
NGC4214	0	0	-12.321	-0.623	0.612	-1.141	2.268	-1.495	2.546
NGC4217	0	0	-12.524	-0.133	0.152	-0.411	0.531	-0.539	0.917
NGC4389	0	0	-13.362	-0.535	0.500	-4.423	2.018	-8.546	2.272
NGC4559	1	1	-12.948	-0.310	0.233	-0.639	1.072	-0.793	1.142
NGC5005	0	0	-12.797	-0.207	0.230	-0.896	0.622	-1.794	0.806
NGC5033	0	0	-13.178	-0.091	0.093	-0.299	0.275	-0.404	0.358
NGC5055	0	0	-12.868	-0.079	0.075	-0.281	0.182	-0.334	0.196
NGC5371	0	0	-13.852	-0.070	0.070	-0.211	0.206	-0.304	0.270
NGC5585	0	0	-12.534	-0.269	0.379	-0.767	1.088	-0.889	1.280
NGC5907	0	0	-13.390	-0.034	0.045	-0.102	0.130	-0.173	0.195
NGC5985	0	0	-13.822	-0.077	0.071	-0.223	0.221	-0.313	0.326
NGC6015	0	0	-13.542	-0.087	0.091	-0.256	0.276	-0.351	0.395
NGC6195	1	1	-13.115	-0.100	0.117	-0.305	0.339	-0.480	0.500
NGC6503	1	0	-12.825	-0.046	0.043	-0.126	0.145	-0.193	0.201
NGC6674	0	0	-13.527	-0.069	0.090	-0.215	0.258	-0.280	0.342
NGC6789	1	1	-12.319	-0.199	0.367	-0.733	1.125	-1.042	1.775
NGC6946	1	1	-13.061	-0.072	0.126	-0.284	0.306	-0.338	0.413
NGC7331	1	1	-12.781	-0.066	0.062	-0.183	0.212	-0.229	0.280
NGC7793	1	1	-13.295	-0.173	0.242	-0.521	0.815	-0.656	1.117
NGC7814	1	1	-12.574	-0.051	0.061	-0.162	0.176	-0.221	0.249
PGC51017	0	0	-15.216	-1.085	0.470	-4.461	0.965	-6.882	1.214
UGC00128	0	0	-14.072	-0.077	0.064	-0.206	0.219	-0.290	0.302
UGC00191	1	0	-13.893	-0.196	0.224	-0.635	0.762	-0.846	1.033
UGC00634	1	1	-13.008	-0.334	0.456	-0.891	1.328	-1.202	1.730
UGC00731	0	0	-12.713	-0.311	0.414	-0.725	1.446	-0.961	1.637
UGC00891	0	0	-12.596	-0.281	0.360	-0.786	1.046	-0.878	1.264
UGC01230	0	0	-15.361	-1.078	0.620	-4.471	1.723	-6.543	3.843
UGC01281	1	1	-12.995	-0.068	0.089	-0.232	0.236	-0.317	0.388
UGC02023	0	0	-13.451	-1.422	1.065	-5.055	3.715	-9.058	4.461
UGC02259	0	0	-13.623	-0.290	0.251	-0.810	0.954	-1.063	1.199
UGC02455	0	0	-13.292	-0.463	0.337	-4.016	1.699	-6.695	2.232
UGC02487	0	0	-13.467	-0.046	0.084	-0.182	0.214	-0.271	0.282
UGC02885	1	1	-13.002	-0.076	0.110	-0.251	0.318	-0.389	0.475
UGC02916	0	0	-13.616	-0.203	0.263	-0.829	0.803	-1.081	0.884
UGC02953	0	0	-12.976	-0.057	0.054	-0.151	0.144	-0.175	0.168
UGC03205	0	0	-13.227	-0.080	0.060	-0.240	0.193	-0.301	0.246
UGC03546	1	1	-12.919	-0.134	0.093	-0.378	0.332	-0.447	0.504
UGC03580	0	0	-12.360	-0.326	0.216	-0.640	0.722	-0.703	0.859
UGC04278	1	0	-12.650	-0.277	0.400	-0.606	1.810	-0.832	1.853
UGC04305	0	0	-15.526	-0.973	0.731	-4.201	1.836	-7.082	2.361
UGC04325	0	0	-13.041	-0.295	0.362	-2.365	1.335	-3.097	1.391
UGC04483	1	1	-13.411	-0.117	0.156	-0.398	0.439	-0.583	0.607
UGC04499	1	1	-13.303	-0.251	0.367	-0.767	1.270	-1.073	1.543
UGC05005	1	1	-13.166	-0.496	0.397	-1.148	1.735	-1.641	2.361
UGC05253	0	0	-12.753	-0.075	0.071	-0.224	0.203	-0.285	0.273
UGC05414	1	1	-13.189	-0.337	0.309	-0.844	1.227	-1.338	1.509
UGC05716	0	0	-13.871	-0.191	0.176	-0.498	0.651	-0.730	0.823
UGC05721	1	1	-12.669	-0.212	0.262	-0.541	0.851	-0.727	1.047
UGC05750	1	1	-13.314	-0.301	0.269	-0.789	1.062	-1.187	1.708
UGC05764	0	0	-12.945	-0.343	0.272	-0.760	0.932	-0.912	1.114

Table A1 – *continued*

Galaxy	P_5	P_3	$\log_{10} a_0$	$1\sigma_-$	$1\sigma_+$	$3\sigma_-$	$3\sigma_+$	$5\sigma_-$	$5\sigma_+$
UGC05829	1	1	-13.084	-0.490	0.710	-1.400	2.278	-2.139	3.078
UGC05918	1	1	-13.150	-0.270	0.429	-0.842	1.481	-1.234	1.775
UGC05986	1	0	-12.549	-0.187	0.343	-0.495	1.267	-0.702	1.899
UGC05999	0	0	-13.264	-0.514	1.090	-1.752	2.995	-2.707	3.309
UGC06399	1	1	-12.859	-0.154	0.164	-0.449	0.545	-0.590	0.849
UGC06446	1	1	-13.054	-0.280	0.270	-0.732	1.182	-1.033	1.369
UGC06614	1	1	-12.537	-0.376	0.422	-0.941	1.569	-1.098	1.870
UGC06628	0	0	-14.446	-1.440	1.302	-4.975	4.232	-6.976	5.263
UGC06667	1	0	-12.523	-0.135	0.137	-0.357	0.491	-0.463	0.724
UGC06786	1	1	-12.094	-0.163	0.107	-0.385	0.335	-0.449	0.432
UGC06787	0	0	-13.461	-0.051	0.054	-0.137	0.261	-0.172	0.320
UGC06818	1	0	-12.939	-0.182	0.392	-0.603	0.832	-0.817	1.176
UGC06917	1	1	-12.850	-0.196	0.130	-0.511	0.506	-0.784	0.753
UGC06923	1	1	-13.060	-0.172	0.211	-0.562	0.645	-0.857	0.966
UGC06930	1	1	-13.393	-0.295	0.387	-1.037	1.194	-1.468	1.794
UGC06973	0	0	-12.023	-0.146	0.144	-0.395	0.519	-0.505	0.789
UGC06983	1	1	-12.982	-0.115	0.173	-0.390	0.511	-0.488	1.086
UGC07089	1	1	-13.306	-0.199	0.179	-0.563	0.642	-0.819	1.001
UGC07125	1	1	-13.994	-0.239	0.326	-0.707	1.130	-1.206	1.474
UGC07151	1	1	-13.162	-0.109	0.076	-0.300	0.261	-0.432	0.353
UGC07232	0	0	-12.844	-0.205	0.188	-0.616	0.622	-1.084	0.753
UGC07261	1	1	-13.324	-0.550	0.724	-1.986	2.281	-2.765	2.878
UGC07323	1	1	-13.170	-0.337	0.399	-1.111	1.358	-2.012	1.646
UGC07399	1	1	-12.322	-0.254	0.257	-0.567	1.019	-0.816	1.174
UGC07524	1	1	-13.248	-0.101	0.149	-0.334	0.424	-0.445	0.640
UGC07559	0	0	-13.615	-0.154	0.155	-0.494	0.460	-0.771	0.582
UGC07577	0	0	-14.543	-0.554	0.349	-4.359	0.746	-7.555	0.934
UGC07603	1	1	-12.579	-0.248	0.321	-0.567	1.118	-0.798	1.248
UGC07608	0	0	-12.930	-0.555	0.811	-1.611	2.950	-3.897	3.455
UGC07690	1	1	-13.545	-0.353	0.387	-1.243	1.402	-3.547	2.267
UGC07866	0	0	-13.450	-0.269	0.227	-0.835	0.778	-1.358	1.305
UGC08286	1	0	-12.865	-0.049	0.043	-0.139	0.138	-0.189	0.181
UGC08490	1	1	-12.974	-0.121	0.122	-0.335	0.392	-0.472	0.576
UGC08550	1	1	-13.104	-0.171	0.334	-0.509	1.043	-0.719	1.225
UGC08699	1	1	-12.986	-0.100	0.162	-0.339	0.434	-0.442	0.586
UGC08837	0	0	-13.517	-0.170	0.118	-0.487	0.364	-0.764	0.489
UGC09037	1	1	-12.870	-0.148	0.122	-0.394	0.419	-0.512	0.679
UGC09133	0	0	-13.289	-0.045	0.050	-0.201	0.141	-0.212	0.188
UGC09992	0	0	-13.884	-1.364	0.951	-5.280	2.972	-7.462	4.018
UGC10310	1	1	-13.353	-0.388	0.607	-1.896	1.914	-2.739	2.241
UGC11455	0	0	-12.855	-0.076	0.113	-0.246	0.334	-0.361	0.441
UGC11557	0	0	-13.319	-0.678	0.791	-3.596	2.781	-6.638	2.982
UGC11820	1	1	-13.164	-0.393	0.304	-0.877	1.064	-1.155	1.202
UGC11914	1	1	-12.183	-0.140	0.096	-0.405	0.311	-0.554	0.385
UGC12506	1	1	-13.345	-0.106	0.128	-0.342	0.360	-0.514	0.535
UGC12632	1	1	-13.466	-0.280	0.332	-0.795	1.161	-1.228	1.385
UGC12732	1	1	-13.441	-0.370	0.374	-0.984	1.201	-1.664	1.476
UGCA281	0	0	-13.149	-0.130	0.115	-0.379	0.368	-0.563	0.541
UGCA442	1	0	-12.839	-0.105	0.198	-0.302	0.617	-0.390	0.793
UGCA444	1	1	-13.272	-0.062	0.091	-0.215	0.257	-0.303	0.402